

## Near-threshold proton-induced neutral pion production from $^{12}\text{C}$

M. A. Pickar

*Department of Physics and Astronomy, University of Kentucky, Lexington, Kentucky 40506*

A. D. Bacher, M. Hugi,\* H. O. Meyer, and R. E. Pollock

*Department of Physics, Indiana University, and Indiana University Cyclotron Facility, Bloomington, Indiana 47405*

G. T. Emery

*Physics Department, Bowdoin College, Brunswick, Maine 04011*

H. J. Karwowski

*Department of Physics and Astronomy, University of North Carolina, Chapel Hill, North Carolina 27514*

J. R. Hall

*Physics Department, University of New Mexico, Albuquerque, New Mexico 87131*

M. Fatyga

*Physics Department, Brookhaven National Laboratory, Upton, New York 11973*

(Received 2 August 1993)

The total cross section and angular distributions for the differential cross section and the analyzing power of the exclusive two-body pion production reaction  $^{12}\text{C}(\bar{p}, \pi^0)^{13}\text{N}_{\text{g.s.}}$  have been measured at 147 MeV, very near the threshold energy of 145 MeV. Both the large forward-backward asymmetry in the angular distribution of the differential cross section and the large values observed for the analyzing powers indicate strong interference between the amplitude for  $s$ -wave pion emission and the amplitudes for  $p$ -wave pion emission. A phase-shift analysis performed on these new data yields significant  $p$ -wave strength at this low energy. The measurements for  $\pi^0$  production from carbon are in agreement with results extracted from existing data for  $\pi^+$  production from carbon, after corrections for isospin invariance and Coulomb effects. The reduced  $s$ -wave strength is found to have a simple power law dependence on the total number of nucleons in the final bound state.

PACS number(s): 25.40.Qa, 24.50.+g, 24.70.+s

### I. INTRODUCTION

While there have been a large number of experimental investigations of proton-induced *charged* pion production from carbon in the threshold region, very few measurements of the *neutral* pion production reaction have been reported. This stems primarily from the fact that the instrumentation and techniques needed to make studies of  $\pi^0$  production are significantly different from those used in detecting charged pions. One group has recently demonstrated the capability of studying  $\pi^0$  production by detecting the associated recoil nucleus [1–4]. In this work we will present results obtained using a technique in which the decay photons of the  $\pi^0$  are detected.

Studies of  $\pi^0$  production have the advantage that they allow one to extend investigations of mechanisms for pro-

ducing pions to energies much closer to threshold than are usually possible when one detects charged pions. Low energy, charged pions have a small probability of surviving the flight paths typical in detectors utilizing magnetic analysis. In addition, Coulomb effects seriously diminish and/or distort the observables in charged-pion production very near threshold, and the manner in which one corrects for Coulomb effects remains an important and difficult problem that must be addressed. Studies of pion production mechanisms using the neutral pion channel provide an effective means of overcoming these obstacles.

Generally, one finds that, at energies not too far above threshold, reaction mechanisms involving the production of an intermediate  $\Delta$  resonance begin to play an important role. To isolate nonresonant reaction mechanisms in proton-induced  $\pi^+$  or  $\pi^0$  production, it is necessary to make measurements very close to the pion production threshold.

There presently exists a substantial body of data very near threshold for the production of pions in a two-body final state for the fundamental reaction  $p + n \rightarrow d + \pi^0$

\*Present address: Colenco Power Consulting Ltd., Mellingerstrasse 207, CH-5405 Baden, Switzerland.

[5–8] and for  $p + d \rightarrow {}^3\text{He} + \pi^0$  [9–12], but comparable data in heavier systems remain scarce. The results presented in this paper represent the lowest energy data in existence for angular distributions of both cross sections and analyzing powers for proton-induced pion production from any target heavier than deuterium.

## II. EXPERIMENTAL METHOD

The experiment was performed at the Indiana University Cyclotron Facility (IUCF), using a polarized proton beam incident on an enriched  ${}^{12}\text{C}$  foil (99.9%, 50 mg/cm<sup>2</sup>). The mean beam energy at the center of the target was 146.87 MeV, and was subject to an absolute uncertainty of  $\pm 0.09$  MeV. The incident beam had a spread in energy, determined by the entrance and exit slits in a 45° analyzing magnet, with a full width of about 0.18 MeV. The energy loss of beam protons traversing the full target thickness was 0.24 MeV. These conditions lead to the production of neutral pions in the reaction  ${}^{12}\text{C}(p, \pi^0){}^{13}\text{N}_{\text{g.s.}}$  with a mean center-of-mass (c.m.) energy  $T_{\pi}^{\text{c.m.}} = 1.65 \pm 0.08$  MeV, with a full width of 0.25 MeV. This corresponds to a velocity parameter

$$\eta \equiv p_{\pi}/m_{\pi}c = 0.157 \pm 0.004,$$

with a full width of 0.012.

The threshold beam energy for this two-body reaction to the ground state of  ${}^{13}\text{N}$  is 144.98 MeV. The next threshold for  $\pi^0$  production from  ${}^{12}\text{C}$  is at 147.11 MeV for the three-body reaction  ${}^{12}\text{C}(p, p\pi^0){}^{12}\text{C}_{\text{g.s.}}$ . The thresholds for *all* other final states are at higher energies. Therefore, if we have a pure  ${}^{12}\text{C}$  target and no background, the beam energy is correct, and the full width of the beam is the 0.18 MeV determined by the slits of the analyzing magnet, then all observed  $\pi^0$ 's in this experiment come from only the transition of interest,  ${}^{12}\text{C}(p, \pi^0){}^{13}\text{N}_{\text{g.s.}}$ . After considering the small uncertainties in the absolute beam energy, the small uncertainties in the details of the energy spectrum of the incident beam, and the small uncertainties in the threshold cross section for  ${}^{12}\text{C}(p, p\pi^0){}^{12}\text{C}_{\text{g.s.}}$ , we conclude that 99±1% of the observed  $\pi^0$ 's in this experiment come from only the transition of interest,  ${}^{12}\text{C}(p, \pi^0){}^{13}\text{N}_{\text{g.s.}}$ .

Background from stray beam striking the target frame, the target chamber, or the beam pipe was determined by making measurements using an empty frame. The background was minimized by using low mass in structures for the target ladder, target chamber, and beam pipe. Special care was also taken in the beam preparation to obtain a clean beam with minimal halo. The background from traces of  ${}^{13}\text{C}$  in our target was estimated to be negligible, based on separate measurements of yields using enriched  ${}^{13}\text{C}$  targets [13].

A sketch illustrating the principal features of the detector geometry is shown in Fig. 1. In this experiment both photons coming from the decay of a  $\pi^0$  were detected in a coincidence between an array of eight independent photon detectors arranged in different angular geometries, one of which is illustrated in Fig. 1. An event consisted of a prompt coincidence between any detector on the left and any detector on the right.

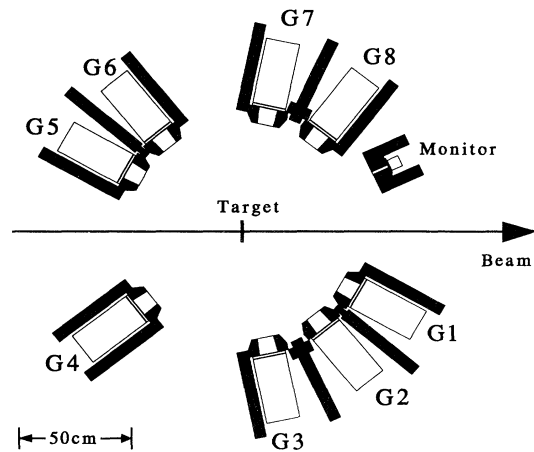


FIG. 1. A sketch showing the principal features of the experimental setup. The incident polarized proton beam passes through an enriched  ${}^{12}\text{C}$  target and terminates in a shielded Faraday cup (not shown). The two photons from the decay of a  $\pi^0$  are detected in a prompt coincidence between a photon detector on the right (G1–G4) and a photon detector on the left (G5–G8). A monitor detector is used to monitor relative luminosity and relative beam polarization.

The photon detectors each consisted of a block of Schott F2 lead glass  $15 \times 15 \times 30$  cm<sup>3</sup>. Attached to each was a fast phototube, 12.7 cm in diameter (Amperex XP2041). The tubes were optically coupled to the glass using a liquid silicon oil of low viscosity (Dow Corning 710) with a refractive index matching the lead glass to the phototube face [14]. The intrinsic efficiency of these counters for photons in the energy range of interest was measured to be 99±1% [14]. Clearly defined broad peaks in pulse height are observed for photons with energies greater than 30 MeV [14–16]. The threshold was set at 15 MeV. Each photon detector had a time resolution of  $\sim 0.8$  ns. The geometric solid angle of each detector was defined by a lead collimator to 20.8 msr. The inner faces of the collimators were sloped toward the target point, to reduce corrections arising from  $\gamma$ -collimator interactions. A photon passing through the collimator aperture could escape the photon detector without interaction only by passing through a minimum of 30 cm of lead glass. A veto Čerenkov counter, of 1-cm-thick plastic, was placed immediately after the collimator in front of each lead glass element. Lead shielding was placed between adjacent detectors to minimize cross talk, and between detectors and the beam line to minimize background.

The incident beam current was typically 60 nA. The resulting rates for real  $\pi^0$ 's detected using a *specific pair* of photon detectors ranged from 10/h to 60/h. Data were accumulated for a total of 8 h, resulting in the collection of 1300 neutral pion events.

For each measurement the pulse height and time-of-flight relative to the cyclotron rf (rf-TOF) were recorded on magnetic tape, event by event, for each photon detector. The electronics was configured so that random coin-

cidence yields could be determined by examining coincidences involving adjacent beam bursts.

Figure 2 shows typical rf-TOF spectra for detector G2 (positioned on the right at  $50.8^\circ$ ). Spectrum 2(a) is the result for G2 in coincidence with *any* detector on the left (opposite) side of the beam. The only constraints are those imposed by the hardwired trigger: a timing window of 60 ns and a pulse height threshold of 15 MeV. The prominent peak (FWHM=1.2 ns) from prompt  $\gamma$  coincidences is clearly visible. Immediately to the right is a small broad bump arising from particle coincidences, which result from the creation of high-energy photons within the lead glass itself by the scattered particles incident on the photon detector. The  $\gamma$  peak and particle bump associated with random coincidences are found one beam burst (30 ns) to the left.

Figure 2(b) shows the spectrum for G2 after imposing more restrictive cuts in the off-line data reduction. In this case there is a higher threshold of 30 MeV on the pulse height of each photon detector, and G2 is required to be in coincidence *only* with G6 (which, in the selected geometry, is almost directly opposite to G2). Finally, a narrow cut is imposed on the rf-TOF of G6, selecting only events in the prompt  $\gamma$  peak. One observes in Fig. 2(b) that the peak for prompt  $\gamma$ 's in G2 is well above the background, as estimated by integrating over the region where the random  $\gamma$  peak occurs. In all of our detector geometries, the random background was less than 15%. Measurements made below threshold gave evidence for

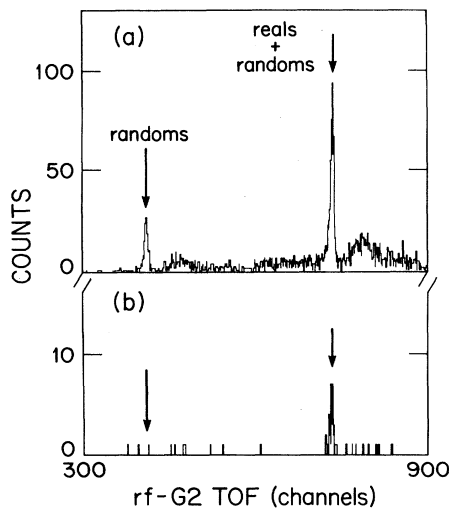


FIG. 2. Representative rf-TOF (time-of-flight) spectra for photon detector G2 positioned on the right at  $50.8^\circ$ . (a) shows the raw data with only the hardware trigger: G2 in coincidence with *any* detector on the left, a pulse height threshold cut of 15 MeV, and a coincidence window of 60 ns. Clearly visible is the prompt  $\gamma$  peak from (reals+randoms), and the  $\gamma$  peak from (randoms) alone. These peaks are separated by one beam burst (30 ns). In (b) we see the result when G2 is in coincidence with G6 alone, a pulse height threshold cut of 30 MeV is applied, and the rf-TOF for G6 is constrained to a narrow window about its (reals+randoms)  $\gamma$  peak.

no events other than the random background.

In addition to the photon detectors used in this experiment, a flux monitor was also employed. This monitor consisted of a particle telescope with a  $\Delta E$  element of plastic scintillator (3.2 mm thick), and an  $E$  detector of NaI ( $\phi$  5.1 cm  $\times$  5.1 cm). The monitor was shielded on all sides with lead, and had a small lead collimator (see Fig. 1). It was positioned at  $25^\circ$  and was configured to detect high-energy protons from the target. It also served to monitor the average relative beam polarization.

The normal component of the beam polarization was measured frequently using  $p$ - $^4\text{He}$  elastic scattering in a polarimeter located between the injector-stage and the main-stage cyclotrons. The beam polarization was typically 0.75 and the spin state of the beam was flipped every 100 s. The normal component of the beam polarization incident on our target is estimated to have a systematic uncertainty of 0.03.

### III. DATA REDUCTION AND ANALYSIS

In general, the energy and direction of a neutral pion can be determined from the directions and energies of its associated decay photons. In this experiment, the c.m. energy of the neutral pion is *fixed* by the incident beam energy because the reaction involves a two-body final state, and only that state is permitted by the conservation of energy. The energy resolution of the photon detectors was insufficient to provide any detailed information on the  $\pi^0$  energy, other than to provide unambiguous identification of neutral pion decay events.

Although each photon detector was unable to provide a precise measurement of the angle of a photon from a single decay event, the limits of angular acceptance for each detector were well defined by its associated lead collimator. This means that the  $\pi^0$  detection efficiency *functions* for any given pair of detectors were well defined, and nonzero over only a restricted range of angles. Because different pairs of detectors are sensitive to different ranges of  $\pi^0$  angles, one can extract angular distributions of the differential cross sections and analyzing powers for the reaction by a statistical analysis of the event record.

In Fig. 3 the efficiency functions for three symmetric pairs of photon detectors positioned at lab angles of  $\pm 78.1^\circ$ ,  $\pm 87.5^\circ$ , and  $\pm 96.8^\circ$  are illustrated. These three detector geometries effectively isolate three independent regions for the c.m. angle, centered around  $0^\circ$ ,  $90^\circ$ , and  $180^\circ$ , respectively. The geometries providing sensitivity to the  $0^\circ$  and  $180^\circ$  regions are those accepting gamma ray pairs whose relative angle is close to the *minimum* allowed. In contrast, the symmetric geometry providing sensitivity to the  $90^\circ$  region is one for which the relative angle between the two accepted gamma rays is close to  $180^\circ$ .

By making use of nonsymmetric pairs of photon detectors, other angular regions can be sampled. In addition, such asymmetric detector pairs permit one to sample events on one side of the beam with a significantly higher weight than on the other side. This provides one with the capability of measuring analyzing powers for the reaction for angular distributions of limited complexity.

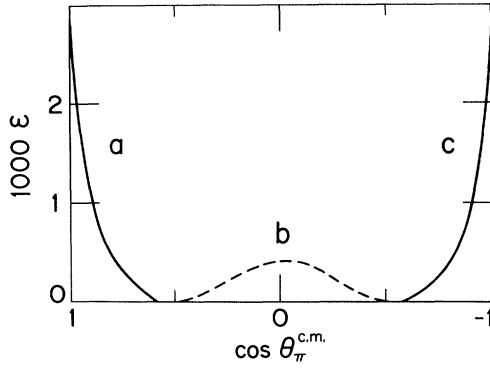


FIG. 3. The projected efficiency functions for a symmetric pair of detectors positioned at  $\pm 78.1^\circ$  [the solid curve (a) peaking at  $0^\circ$ ], at  $\pm 87.5^\circ$  [the dashed curve (b) peaking at about  $90^\circ$ ], and at  $\pm 96.8^\circ$  [the solid curve (c) peaking at  $180^\circ$ ].

Because each pair of detectors is sensitive to a range of angles, angular distributions have to be determined by a fitting procedure that incorporates assumptions about the maximum degree of complexity possible in the angular distributions. Since this experiment was performed very close to threshold, only a limited number of partial waves are expected to contribute and one can place limits on the expected degree of complexity.

We expand the differential cross section  $d\sigma/d\Omega$  and cross section asymmetry  $A_y(d\sigma/d\Omega)$  in truncated Legendre series,

$$\frac{d\sigma}{d\Omega} = \sum_{l=0}^N a_l P_l(x), \quad (1)$$

$$A_y \frac{d\sigma}{d\Omega} = \sum_{l=1}^N b_l P_l^1(x) \cos\phi. \quad (2)$$

Here  $x \equiv \cos\theta_\pi^{\text{c.m.}}$ ,  $\phi$  is the azimuthal angle of the  $\pi^0$  in the c.m. ( $\phi=0$  corresponds to beam left), and  $P_l(x)$  and  $P_l^1(x)$  are regular and associated Legendre polynomials [17].

If only  $s$ - and  $p$ -wave pion emission (relative to the residual nucleus) are possible, then we expect  $N=2$ . If  $d$ -wave pion emission is possible, then  $N$  increases to 4. The detector geometries for this experiment had sufficient angular sensitivity to make a significant determination of coefficients for distributions that included  $d$ -wave pion emission.

The measured yields are related to the intrinsic angular distributions in Eqs. (1) and (2) by simple integrals over phase space, weighted by the appropriate efficiency function for a given detector pair,  $g(x, \phi)$ :

$$Y_\uparrow = Y + P_\uparrow \Delta Y, \quad (3)$$

$$Y_\downarrow = Y - P_\downarrow \Delta Y, \quad (4)$$

where the reduced yields  $Y$  and  $\Delta Y$  are defined by

$$Y = \int d\Omega \frac{d\sigma}{d\Omega} g(x, \phi) \quad (5)$$

and

$$\Delta Y = \int d\Omega A_y \frac{d\sigma}{d\Omega} \cos\phi g(x, \phi). \quad (6)$$

The quantity  $Y_{\uparrow(\downarrow)}$  is the observed yield with proton spin up (down);  $P_{\uparrow(\downarrow)}$  is the absolute value of the polarization for spin up (down) incident protons;  $x$  is  $\cos\theta_\pi^{\text{c.m.}}$ ;  $\phi$  is the azimuthal angle of the  $\pi^0$  in the c.m. ( $\phi=0$  is beam left); and  $g(x, \phi)$ , the geometrical acceptance, is the probability that a  $\pi^0$  emitted with angular coordinates  $(x, \phi)$  is detected by the given detector pair. This geometrical acceptance was computed for each detector pair using Monte Carlo techniques [9,14].

In each of the previous two formulas everything within the integrals is a known quantity, except the coefficients  $a_l$  and  $b_l$  used to expand the cross section and the cross section asymmetry. We can therefore rewrite the above expressions more simply in terms of effective efficiency factors, as

$$Y \equiv \sum_{l=0}^N a_l \varepsilon_l \quad (7)$$

and

$$\Delta Y \equiv \sum_{l=1}^N b_l \varepsilon_l^*. \quad (8)$$

The efficiency coefficients  $\varepsilon_l$  and  $\varepsilon_l^*$  incorporate all necessary integrations and can be readily calculated for each detector pair:

$$\varepsilon_l \equiv \int d\Omega g(x, \phi) P_l(x), \quad (9)$$

$$\varepsilon_l^* \equiv \int d\Omega \cos\phi g(x, \phi) P_l^1(x). \quad (10)$$

These expressions for each detector pair may be combined to define two independent fitting criteria,

$$\chi_\sigma^2 = \sum_{i=1}^{N_{\text{pair}}} \left[ \left( Y_i - \sum_{l=0}^N a_l \varepsilon_{il} \right) / \delta Y_i \right]^2 \quad (11)$$

and

$$\chi_{\sigma A}^2 = \sum_{i=1}^{M_{\text{pair}}} \left[ \left( \Delta Y_i - \sum_{l=1}^N b_l \varepsilon_{il}^* \right) / \delta \Delta Y_i \right]^2. \quad (12)$$

In the analysis procedure we minimize each of these  $\chi^2$  functions separately to obtain values for the coefficients  $a_l$  and  $b_l$ . The method is effective near threshold because the number of partial waves contributing is limited. In this experiment the number  $N_{\text{pair}}$  of useful detector pairs for the determination of  $a_l$  was 7. The number  $M_{\text{pair}}$  of useful pairs for the determination of  $b_l$  was 4 (3 of the 7 detector pair geometries were symmetric about the beam, and therefore provided no information on the cross section asymmetry).

#### IV. RESULTS

The reduced yields were fit for increasing values of  $N$  and the results are tabulated in Tables I and II. The error quoted for each coefficient is from the diagonal ele-

TABLE I. Fits of the spin-independent yields to a truncated series expansion in Legendre polynomials of the differential cross section,  $d\sigma/d\Omega = \sum_{l=0}^N a_l P_l$ .  $\chi^2_\nu$  is the  $\chi^2$  per degree of freedom. The number of data points was 7 for all of the fits. The errors quoted for the coefficients are obtained from the diagonal elements of the error matrix associated with the fit. The recommended solution (shown bracketed by lines) is that for which  $N=2$ , as there is no evidence for a significant  $d$ -wave contribution in  $a_3$  or  $a_4$ . Note the stability in the different values of  $a_l$  as  $N$  is varied.

$N$	$\chi^2_\nu$	$a_0$ (nb/sr)	$a_1$ (nb/sr)	$a_2$ (nb/sr)	$a_3$ (nb/sr)	$a_4$ (nb/sr)
0	34.34	5.17±0.19				
1	4.18	6.42±0.21	5.26±0.39			
2	0.82	5.83±0.25	5.79±0.41	2.93±0.70		
3	1.04	5.85±0.26	5.72±0.44	3.05±0.75	0.54±1.30	
4	1.38	5.85±0.26	5.69±0.45	3.20±0.79	0.57±1.30	-0.80±1.36

ment of the error matrix associated with the fit to the reduced yields. One observes from the values of the  $\chi^2$  per degree of freedom ( $\chi^2_\nu$ ) that there is no evidence from this experiment for significant terms beyond  $N=2$ . We therefore take the best values of the coefficients to be those for  $N=2$ .

In Fig. 4 the differential cross section resulting from this best fit to the measured yields is plotted as a function of  $\cos\theta_\pi^{\text{c.m.}}$  (solid curve). The one standard deviation bounds of statistical uncertainty of the differential cross section are indicated by the dashed curves. The differential cross section is very forward peaked even at this low energy. It drops from a maximum of 14.5 nb/sr at  $0^\circ$  to a shallow minimum of 2.5 nb/sr at  $130^\circ$ .

In Fig. 5 the cross section asymmetry divided by  $\sin\theta_\pi^{\text{c.m.}}$ ,  $A_y(d\sigma/d\Omega)/\sin\theta$ , is plotted as a function of  $\cos\theta_\pi^{\text{c.m.}}$  (solid curve), with the one standard deviation bounds of statistical uncertainty indicated by the dashed curves.

The analyzing power  $A_y$  shown in Fig. 6 (solid curve) is obtained by dividing the cross section asymmetry by

the differential cross section. The dashed lines indicate the one standard deviation bounds of statistical uncertainty. We find that the analyzing power is large and negative at this low energy, reaching a value of  $-0.65\pm0.20$  at  $114^\circ$ . One should note that our associated Legendre polynomials are defined such that a positive  $b_1$  yields a negative  $A_y$ .

The total cross section for this reaction is obtained from the coefficient  $a_0$ , and amounts to  $\sigma_{\text{tot}} = 4\pi a_0 = 73.2 \pm 3.2$  nb.

All of the uncertainties quoted above for the coefficients, the resulting angular distributions, and the total cross section are purely statistical. There is an additional systematic uncertainty of 10% in the absolute normalization of the cross sections arising from uncertainties in the target thickness (8%), the efficiency of beam current integration (4%), and the computed geometrical acceptance of each photon detector pair (5%). The analyzing powers also have an overall systematic uncertainty of 5% arising from uncertainties in the absolute polarization of the beam.

TABLE II. Fits of the spin-dependent yields to a truncated series expansion in Legendre polynomials of the product of analyzing power and differential cross section,  $A_y(d\sigma/d\Omega) = \sum_{l=1}^N b_l P_l^1$ .  $\chi^2_\nu$  is the  $\chi^2$  per degree of freedom. The number of data points was 4 for all of the fits. The errors quoted for the coefficients are obtained from the diagonal elements of the error matrix associated with the fit. The recommended solution (shown bracketed by lines) is that for which  $N=2$ . The first entry (indicated as  $N=0$ ) provides the  $\chi^2$  obtained if it is assumed that  $A_y=0$  everywhere. The values for  $b_l$  tabulated below yield negative analyzing powers.

$N$	$\chi^2_\nu$	$b_1$ (nb/sr)	$b_2$ (nb/sr)	$b_3$ (nb/sr)
0	5.00	0		
1	0.77	2.25±0.54		
2	0.63	2.32±0.54	0.28±0.27	
3	1.15	2.59±0.99	0.17±0.41	-0.32±0.99

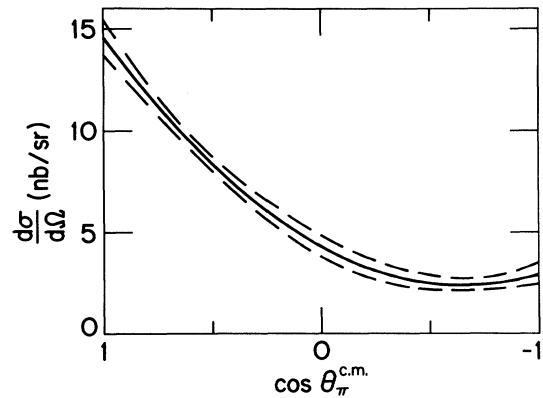


FIG. 4. The differential cross section  $d\sigma/d\Omega$  resulting from the full analysis of the data (solid curve). The dashed lines indicate the one standard deviation bounds of statistical uncertainty.

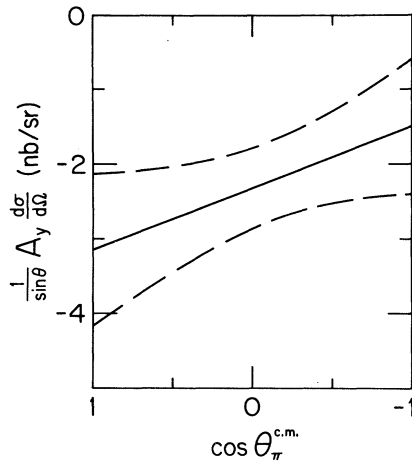


FIG. 5. The product of differential cross section and analyzing power divided by  $\sin\theta$ ,  $A_y(d\sigma/d\Omega)/\sin\theta$ , resulting from the full analysis of the data (solid curve). The dashed lines indicate the one standard deviation bounds of statistical uncertainty. Note that this quantity is everywhere negative.

## V. DISCUSSION

### A. The total cross section

This work represents the lowest energy at which the reaction  $^{12}\text{C}(p, \pi^0)^{13}\text{N}_{\text{g.s.}}$  has been studied ( $T_{\pi}^{\text{c.m.}} = 1.65$  MeV,  $\eta = 0.157$ ). Cross section measurements have recently been published for this reaction which extend to higher energies [1]. The result of this work (solid circle) is plotted as  $\sigma_{\text{tot}}/\eta$  as a function of  $\eta$  in Fig. 7, along with the higher energy  $\pi^0$  results of Ref. [1] (open circles).

There also exists a substantial body of data for the related reaction  $^{12}\text{C}(p, \pi^+)^{13}\text{C}_{\text{g.s.}}$  near the threshold energy [19–24]. Neglecting Coulomb effects, charge indepen-

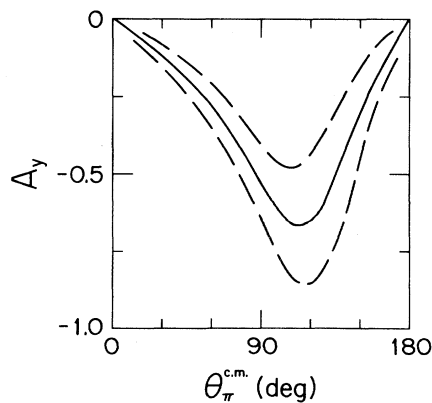


FIG. 6. The analyzing power  $A_y$ , resulting from the full analysis of the data (solid curve). The dashed lines indicate the one standard deviation bounds of statistical uncertainty. Note that  $A_y$  is everywhere negative.

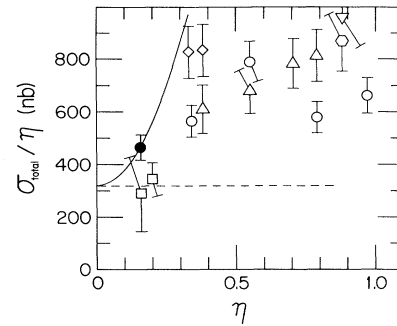


FIG. 7. Variation of  $\sigma_{\text{tot}}/\eta$  with  $\eta \equiv p_{\pi}^{\text{c.m.}}/m_{\pi}c$  for  $p + ^{12}\text{C} \rightarrow ^{13}\text{N}_{\text{g.s.}} + \pi^0$  in the threshold region. The solid circle is from this work, and the open circles are from Ref. [1]. The remaining points are from studies of  $p + ^{12}\text{C} \rightarrow ^{13}\text{C}_{\text{g.s.}} + \pi^+$ , after division by a factor of 2 (as dictated by charge independence), and appropriate Coulomb corrections [18] (see Table III for details). Open squares are from Ref. [19], open diamonds are from Refs. [21, 22], open triangles are from Ref. [23], the open hexagon is from Ref [20], and the open inverted triangle is from Ref. [24]. The systematic uncertainties have been included in the error bars. The dashed line indicates the contribution made by the production of  $s$ -wave pions for the case in which the momentum dependence of the cross section is determined by phase space. The solid curve indicates the combined contributions of  $s$ - and  $p$ -wave pions in the same limit. Both curves were obtained using the results of a phase-shift analysis of this work (see text).

dence predicts  $\sigma_{\pi^+} = 2 \times \sigma_{\pi^0}$  for this reaction pair. In Fig. 7 are plotted the  $\pi^+$  results,  $(\sigma_{\text{tot}}^{\pi^+}/2)/\eta$ , after making a Coulomb correction [18], in which the Coulomb wave functions are evaluated at the surface of the nucleus (open squares [19], open hexagon [20], open diamonds [21, 22], open triangles [23], and open inverted triangle [24]).

All of the  $\pi^+$  results plotted in Fig. 7, with the exception of those of Ref. [19] and the lowest energy point of Ref. [23], were obtained directly by the authors of the present work by fitting the original data for differential cross sections to Legendre expansions. In each case we expanded the series until the  $\chi^2$  reached a reasonably low value, and the analysis showed little sensitivity to the inclusion of higher order terms. The stability of the extracted values of  $\sigma_{\text{tot}} (= 4\pi a_0)$  was also examined for convergence, and for an estimate of the uncertainty from the fitting procedure. The results of our reanalysis of these data are summarized in column 3 of Table III, which lists total cross sections (with no adjustments) for data on this reaction at bombarding energies less than 200 MeV. Some of our results differ from those quoted in other analyses of these same  $\pi^+$  data sets [1, 21, 23].

The results for total cross sections in  $^{12}\text{C}(p, \pi^+)^{13}\text{C}_{\text{g.s.}}$  summarized by Green [23] and again by Homolka *et al.* [1] were obtained from an unpublished phase-shift analysis made by Green [23]. We find that the total cross sections obtained by Green [23] and by Homolka *et al.* [1] using these phase shifts are significantly smaller than the total cross sections obtained by direct fits of the data to a Legendre expansion (the procedure used in our work). We were unable to determine the source of this

TABLE III. A listing of total cross sections for  $^{12}\text{C}(p, \pi^0)^{13}\text{N}_{\text{g.s.}}$  and the related reaction  $^{12}\text{C}(p, \pi^+)^{13}\text{C}_{\text{g.s.}}$  for beam energies less than 200 MeV. Column 3 lists the total cross section,  $\sigma_{\text{tot}}$ , while column 9 lists the reduced cross section obtained after making the appropriate corrections to convert the  $\pi^+$  measurement to the associated  $\pi^0$  result. The reduced total cross sections (in column 9) are obtained by dividing the total cross section (in column 3) by the isospin factor (in column 4) and by the effective Coulomb correction  $C_{\text{eff}}$  (in column 8). Also listed are the Coulomb corrections for the various partial cross sections for the different pion partial waves, to indicate the range of uncertainty in  $C_{\text{eff}}$ . The total cross sections listed in the last eight rows were obtained by the authors of this work after performing a reanalysis of the differential cross section data of Refs. [20–24]. In columns 3 and 9 the first uncertainty listed is statistical, and the second is the estimated systematic uncertainty.

$\eta$	Data type	$\sigma_{\text{tot}}$ (nb)	Isospin factor	$C_{l=0}$	$C_{l=1}$	$C_{l=2}$	$C_{\text{eff}}$	Reduced $\sigma_{\text{tot}}$ (nb)	Source
0.157	$\pi^0$	$73.2 \pm 3 \pm 7$	1	1	1	1	1	$73.2 \pm 3 \pm 7$	(This work)
0.34	$\pi^0$	$192 \pm 8 \pm 19$	1	1	1	1	1	$192 \pm 8 \pm 19$	[1]
0.55	$\pi^0$	$434 \pm 12 \pm 43$	1	1	1	1	1	$434 \pm 12 \pm 43$	[1]
0.79	$\pi^0$	$458 \pm 22 \pm 46$	1	1	1	1	1	$458 \pm 22 \pm 46$	[1]
0.97	$\pi^0$	$643 \pm 31 \pm 64$	1	1	1	1	1	$643 \pm 31 \pm 64$	[1]
0.16	$\pi^+$	$50 \pm 25 \pm 5$	2	0.561	0.486	0.474	0.54	$46 \pm 23 \pm 5$	[19]
0.20	$\pi^+$	$85 \pm 14 \pm 9$	2	0.644	0.580	0.565	0.62	$69 \pm 11 \pm 7$	[19]
0.33	$\pi^+$	$420 \pm 15 \pm 50$	2	0.772	0.764	0.749	0.77	$273 \pm 10 \pm 33$	[21,22]
0.38	$\pi^+$	$506 \pm 8 \pm 61$	2	0.792	0.802	0.789	0.80	$317 \pm 5 \pm 38$	[21,22]
0.38	$\pi^+$	$370 \pm 10 \pm 74$	2	0.792	0.802	0.789	0.80	$232 \pm 6 \pm 46$	[23]
0.55	$\pi^+$	$635 \pm 4 \pm 76$	2	0.817	0.860	0.861	0.85	$374 \pm 3 \pm 45$	[23]
0.71	$\pi^+$	$942 \pm 6 \pm 113$	2	0.816	0.871	0.873	0.85	$554 \pm 4 \pm 66$	[23]
0.78	$\pi^+$	$1093 \pm 15 \pm 131$	2	0.812	0.870	0.866	0.85	$643 \pm 9 \pm 77$	[23]
0.88	$\pi^+$	$1320 \pm 55 \pm 200$	2	0.804	0.868	0.853	0.86	$767 \pm 32 \pm 116$	[20]
0.88	$\pi^+$	$1450 \pm 15 \pm 217$	2	0.804	0.868	0.853	0.86	$843 \pm 9 \pm 126$	[24]

discrepancy, which we have verified as arising from the tabulated phase shifts of Green [23]. The large difference between  $\pi^+$  and  $\pi^0$  total cross sections at  $\eta=0.55$  reported by Homolka *et al.* [1] is not supported by our reanalysis of the  $\pi^+$  data (see Table III and Fig. 7).

The total cross section reported by Soga *et al.* [21] for  $^{12}\text{C}(p, \pi^+)^{13}\text{C}_{\text{g.s.}}$  at  $T_p=200$  MeV ( $\eta=0.88$ ) was obtained by fitting the data of Höistad *et al.* [20] to a Legendre expansion. The value they obtain is smaller than the value we obtain upon reanalysis of the same data set. We find we can reproduce their result if we truncate the Legendre expansion to  $P_3$ . Our analysis, however, indicates a significant reduction in  $\chi^2$  per degree of freedom, and a significant increase in total cross section, if the expansion is continued up through  $P_5$ . This result is confirmed by our analysis of the new data obtained by Korkmaz *et al.* [24] (see Table III and Fig. 7).

Included in Table III are the various factors used to convert each  $\pi^+$  result to the result expected in a reaction producing a  $\pi^0$ . Column 4 lists the factor needed from charge independence. Columns 5, 6, and 7 list the Coulomb corrections needed to convert the cross section of each partial wave strength ( $l=0, 1, \text{ and } 2$ , respectively), if they could be extracted. In column 8 is listed what was taken to be the effective Coulomb correction. In column 9 is listed the reduced total cross section, which is obtained by dividing the total cross section listed in column 3 by the factors tabulated in column 4 (charge independence) and column 9 (Coulomb correction). This reduced total cross section is the quantity plotted in Fig. 7.

The result of the present experiment is in agreement with the low energy  $\pi^+$  results of Marrs, Pollock, and Jacobs [19] (open squares). The result of our experiment

is also in agreement with the trend of the higher energy  $\pi^+$  data. Note that the values of  $\sigma_{\text{tot}}/\eta$  for the  $\pi^+$  experiments do not differ significantly from the  $\pi^0$  measurements of Homolka *et al.* [1]. We see no evidence for a violation of charge independence.

One aspect of importance that can be seen in Fig. 7 is the fair degree of consistency between the results from seven independent experiments using six different techniques. The new low energy point provided by our work supports a tendency for  $\sigma_{\text{tot}}/\eta$  to slowly decrease as  $\eta$  decreases. This is consistent with the expected diminishment of pion  $p$ -wave (and higher-wave) emission due to the centrifugal barrier at low pion energies.

Figure 7 also indicates that  $\sigma_{\text{tot}}/\eta$  increases much more slowly with  $\eta$  than would be expected if the momentum dependence of  $\sigma_{\text{tot}}$  were determined only by phase-space factors. The dashed line shows the expected momentum dependence in this simple phase-space model if only  $s$ -wave pion production contributes. The solid curve shows the expected momentum dependence if both  $s$ - and  $p$ -wave pion production contribute. Both curves are normalized to the results of a phase-shift analysis of our measurements (see Sec. VB). The data indicate that the total cross section clearly departs from the phase-space expectation for  $\eta$  greater than 0.5, and may depart from the phase-space expectation for  $\eta$  as small as 0.3.

A similar result is found for the case of  $^2\text{H}(p, \pi^0)^3\text{He}$  [9]. In that case it is observed that the data depart from the phase-space expectation for  $\eta$  as low as 0.2. One also finds the shapes of the excitation curves ( $\sigma/\eta$  versus  $\eta$ ) to be very similar in the two cases. Both attain a broad maximum in the vicinity of  $\eta \sim 0.8$ , and the ratio of the maximum value attained to that at  $\eta=0$  is approximately 2 in both cases. This is strikingly different from what is

observed in the fundamental reaction  $n + p \rightarrow d + \pi^0$ , whose excitation function peaks at  $\eta = 1.5$  and which has a ratio of peak to zero values amounting to  $\sim 11$  (see the solid curve in Fig. 11 of Ref. [9]).

### B. Phase-shift analysis

The large forward-backward asymmetry observed in the differential cross section and the large analyzing powers provide *direct* experimental evidence that other partial waves besides  $s$ -wave pion emission play a substantial role in  $\pi^0$  production even at the very low energy of this work. Because of the simplicity of the spin structure for the reaction  $p + {}^{12}\text{C} \rightarrow \pi^0 + {}^{13}\text{N}_{\text{g.s.}}$  ( $\frac{1}{2}^+ + 0^+ \rightarrow 0^- + \frac{1}{2}^-$ ), one can perform a phase-shift analysis making use of differential cross section  $d\sigma/d\Omega$  and analyzing power  $A_y$  measurements and extract the  $s$ -wave strength.

The completeness of the analysis is, of course, limited by the data available. To determine the complex amplitudes up through a pion partial wave of  $L_{\text{max}}$  requires measurements of  $d\sigma/d\Omega$  and  $A_y$  at  $2L_{\text{max}} + 2$ , or more, angles. While the number of measurements obtained in this experiment limits our sensitivity to  $L_{\text{max}} = 2$ , fits to the measurements indicate no measurable contribution by partial waves with the  $L > 1$ . We therefore limited ourselves to a phase-shift analysis including only  $s$ - and  $p$ -wave amplitudes.

For this reaction there is only one  $s$ -wave amplitude and two  $p$ -wave amplitudes. One must therefore determine three magnitudes and two relative phases. We have performed the phase-shift analysis using the measured yields directly.

We obtain an  $s$ -wave pion partial cross section  $\sigma_s = 50 \pm 8$  nb. Since the total cross section is  $73.2 \pm 3.2$  nb, we find that  $(32 \pm 10)\%$  of the production strength is  $p$  wave, even at the low energy of this measurement ( $\eta = 0.157$ ,  $T_{\pi}^{\text{c.m.}} = 1.65$  MeV).

This result can be compared to that obtained for  $p + n \rightarrow d + \pi^0$  [7], where the  $p$ -wave strength constitutes  $(13 \pm 2)\%$  of the total cross section at  $\eta = 0.16$ . For the reaction  $p + d \rightarrow {}^3\text{He} + \pi^0$ , the  $p$ -wave strength constitutes  $(16 \pm 10)\%$  of the total cross section at  $\eta = 0.16$  [9].

The increase in the relative  $p$ -wave strength in  ${}^{12}\text{C}(p, \pi^0){}^{13}\text{N}_{\text{g.s.}}$  may be attributed in part to the increased size of the target nucleus. It should be noted, however, that angular momentum and parity conservation force  $s$ -wave pions in this reaction to be produced *only* by incoming protons with  $l_p = 0$ . In the other two reactions on the lightest targets,  $s$ -wave pions can be produced *only* by incoming protons with  $l_p = 1$ . This difference might be expected to be of some significance.

### C. Reduced $s$ -wave strength

It is of interest to compare the absolute  $s$ -wave pion strength obtained in this experiment to that obtained from other targets leading to two-body final states. This information has been obtained for only two other cases,  $p + n \rightarrow d + \pi^0$  [7] and  $p + d \rightarrow {}^3\text{He} + \pi^0$  [9].

If we define a dimensionless reduced matrix element  $|M_s|^2$  for the  $s$ -wave strength,

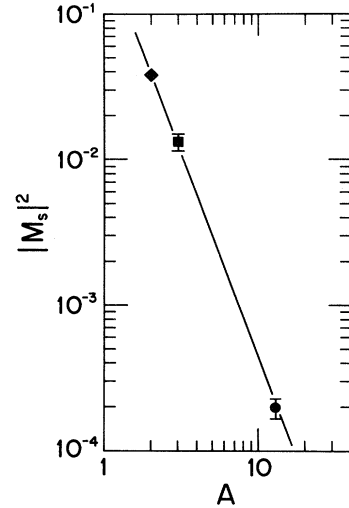


FIG. 8. The variation of the reduced and dimensionless  $s$ -wave strength for pion production,  $|M_s|^2$  (defined in the text), with the *final* nuclear mass  $A$  very near threshold ( $\eta = 0.16$ ). The solid line has the functional dependence  $A^{-2.8}$ . The solid circle is the result of the present work for  ${}^{12}\text{C}(p, \pi^0){}^{13}\text{N}_{\text{g.s.}}$ , the solid square is for  $p + d \rightarrow {}^3\text{He} + \pi^0$  [9], and the solid diamond is for  $p + n \rightarrow d + \pi^0$  [7]. The systematic uncertainties are included in the error bars.

$$\frac{\sigma_s}{\eta} = \frac{1}{k^2} \frac{(2I_3 + 1)(2I_4 + 1)}{(2I_1 + 1)(2I_2 + 1)} |M_s|^2, \quad (13)$$

we can separate out trivial factors arising from phase space and spin multiplicity factors. Here  $k$  is the c.m. momentum of the incoming proton,  $I_1$  and  $I_2$  are the spins of the initial-state particles, and  $I_3$  and  $I_4$  are the spins of the final-state particles.

The resulting values for  $|M_s|^2$  at  $\eta = 0.16$  are shown in Fig. 8. One observes a precipitous drop in strength with *final* nuclear mass  $A$ . The reduced  $s$ -wave strength for  ${}^{12}\text{C}(p, \pi^0){}^{13}\text{N}_{\text{g.s.}}$  is  $\sim 200\times$  smaller than that obtained for the elementary reaction,  $p + n \rightarrow d + \pi^0$ . The data indicate a simple power law dependence for the reduced  $s$ -wave strength. The line drawn in Fig. 8 has a functional dependence of  $A^{-2.8}$ , where  $A$  is the *final* nuclear mass.

## VI. CONCLUSIONS

Angular distributions of the differential cross section and of the analyzing power have been determined for the exclusive reaction  ${}^{12}\text{C}(p, \pi^0){}^{13}\text{N}_{\text{g.s.}}$  at an energy closer to threshold (yielding  $T_{\pi}^{\text{c.m.}} = 1.65$  MeV and  $\eta = 0.157$ ) than has ever been accomplished for *any* ( $N, \pi$ ) study on a target with more than two nucleons. The differential cross section is found to be very forward peaked and the analyzing power is large and negative. This evidence of the large role played by  $p$ -wave amplitudes very near threshold is consistent with that observed in the elementary two-nucleon system,  $n + p \rightarrow d + \pi^0$  [7], and in the three-nucleon system,  ${}^2\text{H}(p, \pi^0){}^3\text{He}$  [9].

A phase-shift analysis of these results permitted an extraction of the  $s$ -wave partial cross section ( $\sigma_s = 50 \pm 8$  nb)

and yielded a relative  $p$ -wave strength of  $(32 \pm 10)\%$ , which is about twice that observed in  $p + n \rightarrow d + \pi^0$  [7] and  $p + d \rightarrow {}^3\text{He} + \pi^0$  [9] at the same value of  $\eta$ .

The reduced  $s$ -wave strength is found to drop precipitously with the mass  $A$  of the final *bound* nuclear system, with an empirical dependence  $\propto A^{-2.8}$ . Because of the large role played by  $p$ -wave emission very near threshold, future studies attempting to explore this dependence will have to be able to reliably isolate the  $s$ -wave strength very near threshold. There are very few spin systems that will permit a meaningful phase-shift analysis using only data for differential cross sections and analyzing powers. One will be forced in most cases to examine the variation of  $\sigma_{\text{tot}}/\eta$  with  $\eta$ , and to assume

$$\lim_{\eta \rightarrow 0} \sigma_{\text{tot}}/\eta = \lim_{\eta \rightarrow 0} \sigma_s/\eta.$$

Studies of the momentum dependence of the reaction  $p + d \rightarrow {}^3\text{He} + \pi^0$  very near threshold [9] indicate that this procedure will be reliable only if measurements are made to *very* small values of  $\eta$  (i.e.,  $\eta < 0.1$ ).

In both  $p + n \rightarrow d + \pi^0$  [7] and  $p + d \rightarrow {}^3\text{He} + \pi^0$  [9]  $\sigma_s/\eta$  is observed to slowly increase as  $\eta$  decreases. In the present work  $\sigma_s/\eta$  was determined at only one value of  $\eta$  ( $\eta = 0.157$ ). The quantity  $\sigma_{\text{tot}}/\eta$  obtained in this experiment, however, can be compared to those obtained in studies of  ${}^{12}\text{C}(p, \pi^+) {}^{13}\text{C}_{\text{g.s.}}$  at nearby and higher energies, after corrections for charge independence and Coulomb

effects, and also to measurements of  ${}^{12}\text{C}(p, \pi^0) {}^{13}\text{N}_{\text{g.s.}}$  made at higher energies. Our result for  $\sigma_{\text{tot}}/\eta$  is in agreement with these other studies, and indicate that  $\sigma_{\text{tot}}/\eta$  is slowly decreasing as  $\eta$  decreases, for  $\eta$  near 0.16. However, if the values for  $\sigma_s/\eta$  for this reaction behave in a manner similar to what is observed in the two lightest nuclear systems, one would expect  $\sigma_{\text{tot}}/\eta$  to begin to *increase* gradually with decreasing  $\eta$  at some value of  $\eta$  below the present value of  $\eta = 0.157$ .

Studies of very near threshold pion production from nuclei are motivated in part by the fact that  $s$ -wave pion production in the elementary reaction  $p + n \rightarrow d + \pi^0$  has no appreciable contribution from terms involving the excitation of an intermediate  $\Delta$ . Since the range probed in this elementary process is smaller than a nucleon diameter, this would imply that near-threshold  $\pi^0$  production may provide a means with which to probe high momentum components of nucleon-nucleon correlations within nuclei. It is hoped that the results provided by this experiment will stimulate future investigations of near-threshold pion production.

#### ACKNOWLEDGMENTS

This work was supported in part by Grant No. NSF PHY-9103794 and Grant No. NSF PHY 81-14339, both from the U.S. National Science Foundation.

- [1] J. Homolka, W. Schott, W. Wagner, W. Wilhelm, M. Saber, R. E. Segel, R. D. Bent, M. Fatyga, R. E. Pollock, P. Kienle, and K. E. Rehm, *Phys. Rev. C* **45**, 1276 (1992).
- [2] J. Homolka, W. Schott, W. Wagner, W. Wilhelm, R. D. Bent, M. Fatyga, R. E. Pollock, M. Saber, R. E. Segel, and P. Kienle, *Phys. Rev. C* **38**, 2686 (1988).
- [3] J. Homolka, W. Schott, W. Wagner, W. Wilhelm, R. D. Bent, M. Fatyga, R. E. Pollock, M. Saber, R. E. Segel, P. Kienle, and K. E. Rehm, *Nucl. Instrum. Methods A* **260**, 418 (1987).
- [4] W. Schott, W. Wagner, P. Kienle, R. Pollock, R. Bent, M. Fatyga, J. Kehayias, M. Green, and K. Rehm, *Phys. Rev. C* **34**, 1406 (1986).
- [5] D. A. Hutcheon, E. Korkmaz, G. A. Moss, R. Abegg, N. E. Davison, G. W. R. Edwards, L. G. Greeniaus, D. Mack, C. A. Miller, W. C. Olsen, I. J. van Heerden, and Ye Yanlin, *Phys. Rev. Lett.* **64**, 176 (1990).
- [6] D. A. Hutcheon, E. Korkmaz, G. A. Moss, R. Abegg, N. E. Davison, G. W. R. Edwards, L. G. Greeniaus, D. Mack, C. A. Miller, W. C. Olsen, I. J. van Heerden, and Y. E. Yanlin, *Nucl. Phys. A* **535**, 618 (1991).
- [7] E. Korkmaz, J. Li, D. A. Hutcheon, R. Abegg, J. B. Elliott, L. G. Greeniaus, D. J. Mack, C. A. Miller, and N. L. Rodning, *Nucl. Phys. A* **535**, 637 (1991).
- [8] B. G. Ritchie, *Phys. Rev. C* **44**, 533 (1991).
- [9] M. A. Pickar, A. D. Bacher, H. O. Meyer, R. E. Pollock, and G. T. Emery, *Phys. Rev. C* **46**, 397 (1992).
- [10] C. Kerboul, A. Boudard, L. Antonuk, J. Arvieux, J. Berger, R. Bertini, M. Boivin, J. M. Durand, A. Stetz, J. Tinsley, J. Yonnet, Nguyen Van Sen, Ye Yanlin, B. Mayer, J. Cameron, C. Lapointe, D. M. Sheppard, J. F. Germond, and C. Wilkin, *Phys. Lett. B* **181**, 28 (1986).
- [11] A. Boudard, C. Kerboul, L. Antonuk, J. Arvieux, J. Berger, R. Bertini, M. Boivin, J. M. Durand, G. Roy, J. Tinsley, J. Yonnet, B. Mayer, and Nguyen Van Sen, *Phys. Lett. B* **214**, 6 (1988).
- [12] F. Plouin, in *Production and Decay of Light Mesons*, edited by P. Fleury (World Scientific, Singapore, 1988), p. 114.
- [13] M. A. Pickar (unpublished).
- [14] M. A. Pickar, Ph.D. thesis, Indiana University, 1982 (unpublished).
- [15] M. A. Pickar, H. J. Karwowski, J. D. Brown, J. R. Hall, M. Hugi, R. E. Pollock, V. R. Cupps, M. Fatyga, and A. D. Bacher, *Phys. Rev. C* **35**, 37 (1987).
- [16] K. W. Pitts, Ph.D. thesis, Indiana University, 1985 (unpublished).
- [17] M. Abramowitz and I. A. Stegun, Eds., *Handbook of Mathematical Functions* (Dover, New York, 1972), p. 334.
- [18] A. Reitan, *Nucl. Phys.* **B11**, 170 (1969).
- [19] R. E. Marrs, R. E. Pollock, and W. W. Jacobs, *Phys. Rev. C* **20**, 2308 (1979).
- [20] B. Höistad, P. H. Pile, T. P. Sjoreen, R. D. Bent, M. C. Green, and F. Soga, *Phys. Lett.* **94B**, 315 (1980).
- [21] F. Soga, P. H. Pile, R. D. Bent, M. C. Green, W. W. Jacobs, T. P. Sjoreen, T. E. Ward, and A. G. Drentje, *Phys. Rev. C* **24**, 570 (1981).
- [22] T. P. Sjoreen, P. H. Pile, R. E. Pollock, W. W. Jacobs, H. O. Meyer, R. D. Bent, M. C. Green, and F. Soga, *Phys. Rev. C* **24**, 1135 (1981).
- [23] M. C. Green, Ph.D. thesis, Indiana University, 1983 (unpublished).
- [24] E. Korkmaz, S. E. Vigdor, W. W. Jacobs, T. G. Throwe, L. C. Bland, M. C. Green, P. L. Jolivet, and J. D. Brown, *Phys. Rev. C* **40**, 813 (1989).